Hindawi Publishing Corporation
Advances in Optical Technologies
Volume 2012, Article ID 765953, 6 pages
doi:10.1155/2012/765953

Research Article

Porosity and Inclusion Detection in CFRP by Infrared Thermography

C. Toscano,[1,2] C. Meola,[3] M. C. Iorio,[3] and G. M. Carlomagno[4]

[1] *C.I.R.A. Italian Aerospace Research Centre, via Maiorise snc, 81043 Capua, Italy*
[2] *Department of Aerospace Engineering, University of Naples Federico II, 80125 Naples, Italy*
[3] *Department of Aerospace Engineering (DIAS), University of Naples Federico II, Via Claudio, 21 80125 Naples, Italy*
[4] *Department of Aerospace Engineering (DIAS), University of Naples Federico II, P.le Tecchio, 21 80125 Naples, Italy*

Correspondence should be addressed to C. Meola, carmeola@unina.it

Received 6 August 2012; Accepted 22 October 2012

Academic Editor: Laura Abbozzo Ronchi

The ever wide use of composite materials in the aeronautical industry has evidenced the need for development of ever more effective nondestructive evaluation methodologies in order to reduce rejected parts and to optimize production costs. Infrared thermography has been recently enclosed amongst the standardized non destructive testing techniques, but its usefulness needs still complete assessment since it can be employed in several different arrangements and for many purposes. In this work, the possibility to detect slag inclusions and porosity is analyzed with both lock-in themography and pulse thermography in the transmission mode. To this end, carbon-fiber-peinforced polymers different specimens are specifically fabricated of several different stacking sequences and with embedded slag inclusions and porosity percentages. As main results, both of the techniques are found definitely able to reveal the presence of the defects above mentioned. Moreover, these techniques could be considered complementary in order to better characterize the nature of the detected defects.

1. Introduction

In the last thirty years a huge employment of carbon-fiber-reinforced polymers (CFRPs) has characterized the production of components in the aerospace industry [1]. Indeed, since their introduction in the civil aviation in the eighties, CFRPs have gained a progressive interest due to their versatility (e.g., perfectly matching the design requirements) as well appreciable low weight and high stiffness with costs saving.

However, due to the many parameters involved in the CFRP manufacturing process, special care must be devoted to production control [2], in order to reduce rejected parts, and to detect, at the onset stage, buried defects, which may, unpredictably, grow once the structure is under load. Moreover, the intrinsic nonhomogeneities of the components and their properties, which are strictly dependent on the fiber quantity and orientation, make them susceptible to damage if impacted, also at low energy. This is why strong efforts have been paid by the industries to develop ever more effective non destructive testing and evaluation techniques [3].

Great attention was devoted, in the last twenty years, to the use of infrared thermography, (IRT) for non destructive evaluation (NDE) of materials and, recently, it was included amongst the standardized NDE techniques in the aeronautical field [4]. The main advantages of IRT are related to its contactless character and fast rate of inspection of large components. It can be used as complement to, or substitute, of the most common techniques.

Infrared thermography for NDE is basically used in the so-called *active* mode [5], which means that the inspected part is heated (or cooled) with respect to the ambient temperature, by an external source. The presence of an inhomogeneity in the inspected material affects the heat propagation and causes a local surface temperature variation. Halogen lamps are mostly used for heating the inspected parts, but also mechanical loading, such as ultrasound waves, could be applied to induce mechanical friction in materials

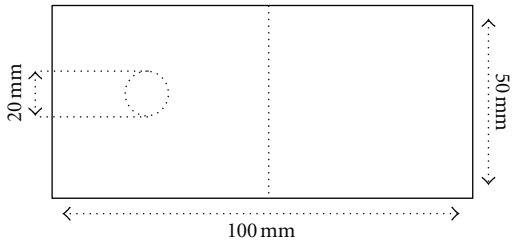

Figure 1: Schematic of the coupon with the Teflon disk embedded.

discontinuities [6]. This causes the generation of heat in the discontinuity, which is revealed by an infrared camera. It has been proven by several authors that infrared thermography is very effective for porosity detection. Amongst the used techniques, the measure of thermal diffusivity, or thermal effusivity, of the material was addressed [7–10].

In this work, CFRP coupons with induced porosity, through the curing cycle and buried slag inclusions are inspected with lock-in Thermography (LT) [11] and Pulse thermography (PT), both used in the transmission mode.

2. Fabrication of CFRP Coupons

A set of coupons was manufactured by hand lay up of prepreg laminas. In order to induce a controlled porosity level, curing in autoclave was performed by applying a temperature-pressure cycle, modified with respect to that suggested by the row material provider. In particular, to generate porosity, just only a partial pressure was used with respect to the prescribed one (7 bar gauge); specifically, a value of 100%, 75%, 50%, 25%, and 0% of the total prescribed pressure was applied during the autoclave curing. For each curing pressure level, four different lamination sequences (see Table 1) were considered in order to study any possible influences the specific fiber alignment may have on the porosity distribution. Therefore, 20 coupons were fabricated (i.e., 4 coupons involving the four different stacking sequences for each curing pressure level).

Moreover, a thin Teflon disk, 20 mm in diameter, was inserted in the middle of the stacking sequence to simulate delamination or inclusion of the bagging film; the thickness of the Teflon disk is of the same order of that of a single prepreg lamina. As sketched in Figure 1, each coupon is 50 mm large and 100 mm long; the thickness may be evaluated owing to the number of plies.

The presence of entrapped gas in the coupons (i.e., porosity), which increases with decreasing the applied pressure, was assessed through density measurements. More specifically, small samples were cut from each type of coupons and subjected to density measurements through the volumetric method (i.e., using a digital balance and the Archimedes plush). The obtained density values are plotted against the curing pressure in Figure 2. As expected, on the whole, the density increases with the pressure.

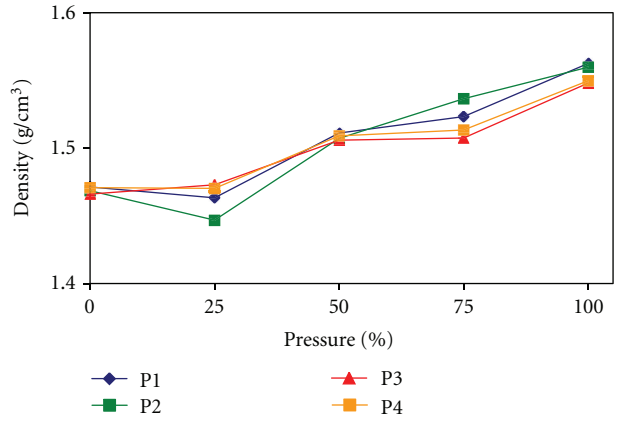

Figure 2: Density values versus the curing pressure percentage (used in autoclave).

3. Inspection with Infrared Thermography

As already stated, the inspection of the manufactured coupons was carried out with LT and PT in the transmission mode; thermal stimulation was performed with a halogen or a flash lamp, respectively. To screen the camera, which is the SC5000 (Flir systems), from the direct intense flash light, coupons were mounted in a proper housing. A test setup is shown in Figure 3; the position of the camera is opposite with respect to that of the lamp.

For LT tests, the infrared camera frames the thermal images and acquires the amplitude/time temperature variations over the rear surface of the coupon. Then, by the provided software, the phase differences between the modulated heating source and the out coming thermal waves are elaborated and represented in false color maps. Of course, the local color variations indicate the presence of inhomogeneities in the material. Then, the presence of the inclusion and/or porosity clusters could be alternately represented with lighter or darker colors in the phase maps. In order to rapidly get an idea about the inner coupons structures, the same excitation frequency was used for testing all the coupons.

The pulse thermography involves a similar test arrangement (Figure 3). The flash lamp is a Hensel MH6000, which is able to emit up to 6000 Joules, and it is driven by a Hensel TRIA6000S power pack producing a flash duration of 1/440 s at the maximum power. The heating of the rear surface of the coupon is recorded by the infrared camera. The time-temperature distribution is characterized by an increase in temperature from the initial one T_i until a maximum T_M is reached, as shown in Figure 4.

It can be demonstrated, under proper hypothesis, that if the surface of a finite slab of a homogeneous material is instantaneously heated up [12], then, if $t = 0$ is the time when the flash is enforced (on the slab opposite side), the instant $t_{1/2}$, corresponding to $T_{M/2}$ (the half of $T_M - T_i$) can

Table 1: Stacking sequences and number of plies of the coupons.

Coupon	Stacking sequence	No. plies
P1	$[0^\circ]$	24
P2	$[90^\circ]$	24
P3	$[(45^\circ/-45^\circ)_6]_S$	24
P4	$[45/0/-45/90/45/0/-45/90//90/-45/0/45/90/-45/0/45]_S$	32

Figure 3: Experimental setup for the lock-in thermography in transmission mode. For the pulsed thermography, the halogen lamp is replaced with the flash lamp.

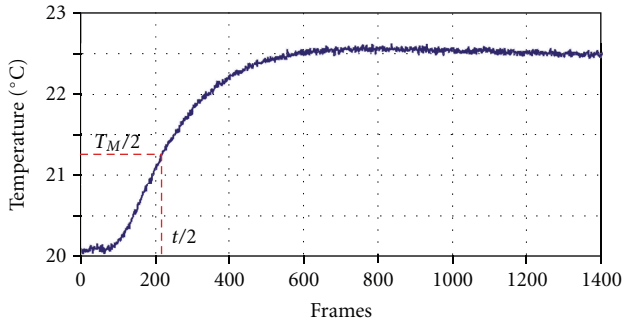

Figure 4: Typical temperature plot during flash heating.

be put in relation with the thermal diffusivity coefficient α and the thickness L of the slab through the following relation:

$$\alpha = \frac{1.38L^2}{\pi^2 t_{1/2}}. \quad (1)$$

Of course, the thermal diffusivity has to be considered as a mean value across each specimen thickness. Thanks to the use of the infrared camera, the thermal "history" of the coupon can be easily recorded and successively analyzed. Then, by neglecting tangential conduction effects, from (1), the thermal diffusivity of the coupon can be calculated point by point over its entire surface. All the calculations, for each coupon, were done by an *ad hoc* tool developed in the Matlab environment, which is able to read the sequence of images accounting for the "thermal history" and to calculate and map the thermal diffusivity.

4. Discussion of Results

In the following Figures 5, 6, 7, 8, and 9 are reported some of the obtained results. For the same coupon, a phase map, obtained by the LT technique, and a thermal diffusivity map, obtained with the Matlab routine from PT sequences, are shown together in the same figure to allow for a direct comparison. In particular, each pair of maps is related to a coupon representing a specific lamination sequence and curing pressure. A color scale with values expressed in 10^{-3} cm^2/s is added to each diffusivity map.

By comparing phase and diffusivity maps, it can be noted, in general, a good matching of data regarding the slag inclusion detection. In particular, from phase maps, it is possible to distinguish not only the buried defects, but also the fiber orientation. On the other side, the map of thermal diffusivity is helpful to better distinguish areas of the material with different thermal behavior. Thus, on the whole, the application of both techniques can lead to a more comprehensive knowledge of the materials inner defects.

However, to a closer view some differences appear, which mainly reside in the position of the detected inclusion. This is due to some differences in the field of view used for the two different tests carried out with LT and PT. In addition, it has to be noted that some phase maps appear quite blurred making difficult distinguishing the Teflon disk; this occurs mainly for the coupon P4 cured at 50% (Figure 7(a)) and the P3 cured at 0% (Figure 9(a)). This is explicable by looking at the diffusivity maps; in fact, it can be noted that the thermal diffusivity in a high porosity area and in the inclusions attains almost the same value, which is smaller than that of the more dense material. Thus, the dampening down of the contrast with decreasing the curing pressure is obviously due a more diffuse presence of porosity, within the whole coupon volume, which masks the thin Teflon disk. This is what happens for the P3 coupon cured at 0% pressure (Figure 9(b)). More difficult to explain appears, at first sight, the poor contrast displayed by the phase map for the coupon P4 at 50% (Figure 7(a)) with respect to that of the coupon P3 at 25% (Figure 8(a)), which, instead, shows a well-contoured defect. However, this may be due to many different factors; the main ones being as follows.

(i) The stacking sequence—the coupon P3 involves fibers at $\pm 45^\circ$, while the P4 one is characterized by the $[45/0/-45/90/45/0/-45/90//90/-45/0/45/90/-45/0/45]_S$ sequence. Of course, the more complex

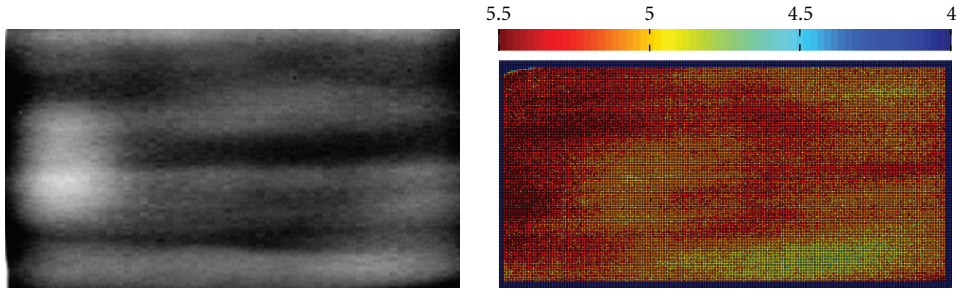

(a) Phase map (b) Diffusivity map

Figure 5: Phase map (a) and diffusivity map (b) of the P1 coupon cured with 100% of the pressure.

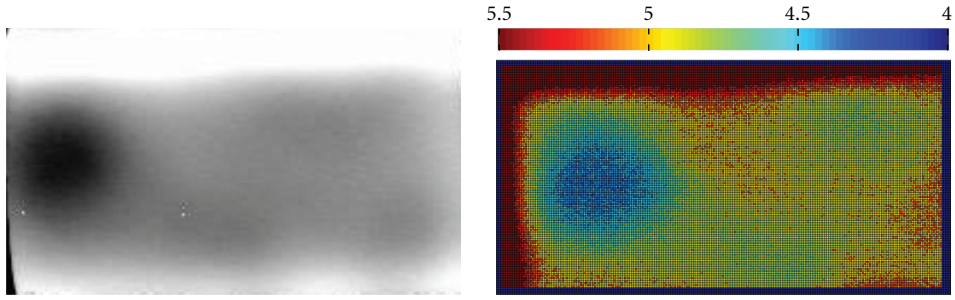

(a) Phase map (b) Diffusivity map

Figure 6: Phase map (a) and diffusivity map (b) of the P3 coupon cured with 75% of the pressure.

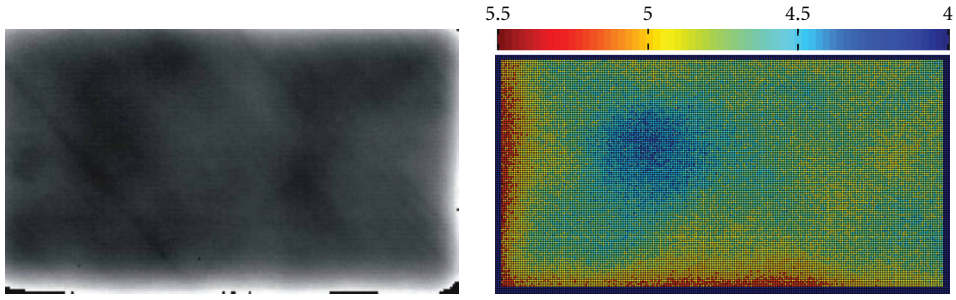

(a) Phase map (b) Diffusivity map

Figure 7: Phase map (a) and diffusivity map (b) of the P4 coupon cured with 50% of the pressure.

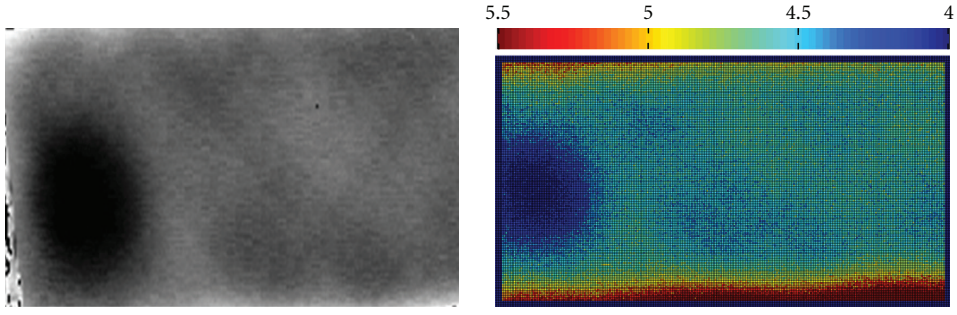

(a) Phase map (b) Diffusivity map

Figure 8: Phase map (a) and diffusivity map (b) of the P3 coupon cured with 25% of the pressure.

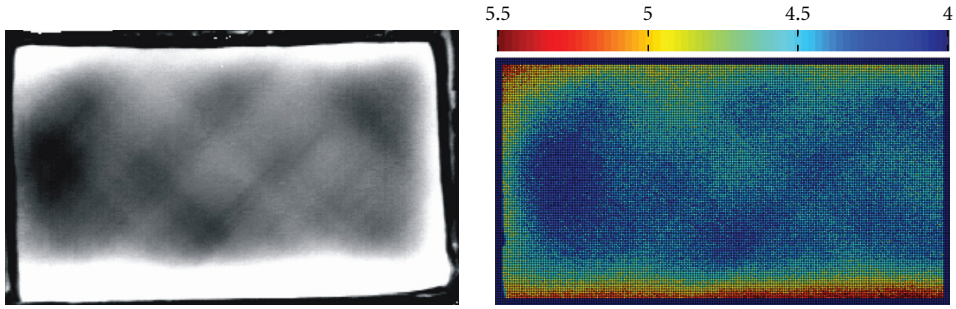

(a) Phase map (b) Diffusivity map

Figure 9: Phase map (a) and diffusivity map (b) of the P3 coupon cured with 0% of the pressure.

stacking sequence hinders the passage of air during application of the vacuum bag, then favouring the formation of air bubbles and of porosity clusters.

(ii) The thickness—the coupon P4 includes a greater number of plies. The contrast generally decreases with increasing the defect depth.

(iii) Manufacturing errors—something wrong is likely to occur during any process.

To better quantify the influence of the curing pressure, an average value α_M of the thermal diffusivity is calculated in a given area relating to the sound half part of the coupon (i.e., the half part without the buried defect). These α_M values are plotted against the curing pressure p_c in Figure 10. As can be seen, the trend of α_M versus p_c is in very good agreement with that of the measured density already shown in Figure 2. By the way, the density is measured by weighting only a very small part of the coupon, while the average thermal diffusivity is measured over a large coupon surface. In the present case, the average was restricted to the coupon sound part (excluding the part with buried the Teflon disk); in a more general way, the thermal diffusivity can be calculated by considering a desired larger area and accounting also for a data deviation to include maxima and minima for a better material characterization. And so, it may be claimed that the indirect porosity estimation, obtained with infrared thermography and the flash method, is more effective and reliable with respect to that measured by the balance method.

As known, thermal diffusivity is higher along the carbon fibers than in the perpendicular direction, where the heat diffusion is principally due to the matrix of the composite. It seems, from Figure 10, that present data, considering data relative to P1 (fibers at 0°) and P2 (fibers at 90°) coupons, are in general agreement with the previous assertion. Instead, data for the P3 and P4 coupons present a quite similar trend, which might mean that, in a complex lamination sequence, the fibers orientation and the number of plies do not have an appreciable influences on the whole trend of the average thermal diffusivity. However, looking at Table 1, it is possible to see that for both P3 and P4 coupons, the external surface is characterized by fibers at 45°; so, this may justify the obtained thermal diffusivity values. On the other side, data obtained

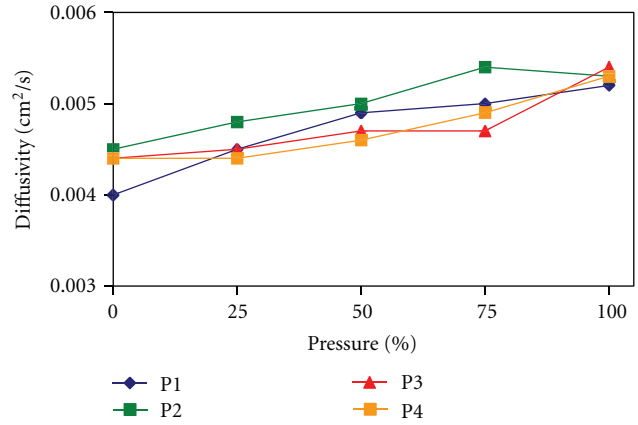

Figure 10: Average diffusivity versus applied curing pressure as percentage of the prescribed one.

with infrared thermography are generally affected by the characteristics of the viewed surface.

5. Conclusion

An experimental investigation was performed in order to gain new information on the application of infrared thermography in the inspection of CFRP for aeronautical use. Several *ad hoc* coupons with both porosity and slag inclusions were fabricated and then inspected with LT and PT techniques; results were presented in terms of phase images and thermal diffusivity maps.

Firstly, results highlight the capability of both techniques to detect the two types of defects. In particular, a smaller diffusivity value was found in a defective zone with respect to the almost homogeneous material. So, the comparison between the phase maps and the diffusivity maps allows gaining more exhaustive and clear information on the nature of the detected inhomogeneities. The obtained results demonstrate the advantage of using both LT and PT in the transmission mode because of the possibility of using the same set-up arrangement for both detection of defects and measurement of thermal diffusivity as well as the possibility for a direct comparison between phase angle and thermal

diffusivity values. In addition, testing in the transmission mode is helpful in the inspection of thick parts, which cannot always be resolved in the reflection mode.

The main drawbacks of both techniques are related to specific experimental conditions. In the case of LT in transmission, proper excitation frequencies must be investigated, as well as their relation with the obtained phase maps, which could lead to improve the knowledge about the porosity distribution and to distinguish inhomogeneities of different nature. Moreover, measurements of thermal diffusivity with PT needs further investigation to improve the signal to noise ratio for more quantitative measurements. What it is clear, is that the two techniques could be combined in order to draw a more clear picture of the conditions of the inspected part.

In the future, these approaches will be deeply investigated in order to define the optimum setup and test parameters so as to enhance the technique ability to detect specific defects and to obtain quantitative information.

Acknowledgment

A special thank goes to Flir systems, Italy, for supplying the Flash lamp.

References

[1] A. A. Baker, S. Dutton, and D. Kelly, *Composite Materials for Aircraft Structures*, AIAA Education Series, 2nd edition, 2004.

[2] http://ntrs.nasa.gov/archive/nasa/casi.ntrs.nasa.gov /20090014807_2009014230.pdf.

[3] C. Beine, C. Boller, U. Netzelmann et al., "NDT for CFRP aeronautical components a comparative study," in *Proceedings of the NDT in Aerospace*, Hamburg, Germany, November 2010.

[4] C. Meola and G. M. Carlomagno, "Infrared thermography in non-destructive inspection: theory and practice," in *Recent Advances in Non Destructive Inspection*, C. Meola, Ed., pp. 89–123, Nova Science Publisher, 2010.

[5] X. Maldague, *Nondestructive Evaluation of Materials by Infrared Thermography*, Springer, New York, NY, USA, 1993.

[6] J. Rantala, D. Wu, A. Salerno, and G. Busse, "Lock-in thermography with mechanical loss angle heating at ultrasonic frequencies," in *Proceedings of the Eurotherm Seminar*, vol. 50, Stuttgart, Germany, September 1996.

[7] E. Grinzato, S. Marinetti, and P. G. Bison, "NDE of porosity in CFRP by multiple thermographic techniques," in *Thermosense XXIV*, vol. 4710 of *Proceedings of SPIE*, pp. 588–598, April 2002.

[8] A. Ciliberto, G. Cavaccini, O. Salvetti et al., "Porosity detection in composite aeronautical structures," *Infrared Physics and Technology*, vol. 43, no. 3-5, pp. 139–143, 2002.

[9] G. Hendorfer, G. Mayr, G. Zauner, M. Haslhofer, and R. Pree, "Quantitative determination of porosity by active thermography," in *Review of Progress in Quantitative Nondestructive Evaluation*, vol. 894, pp. 702–708, August 2006.

[10] G. Mayr and G. Handorfer, "Porosity determination by pulsed thermography in reflection mode," in *Proceedings of the 10th International Conference on Quantitative InfraRed Thermography*, Quebec, Canada, July 2010.

[11] C. Meola, "Nondestructive evaluation of materials with rear heating lock-in thermography," *IEEE Sensors Journal*, vol. 7, no. 10, pp. 1388–1389, 2007.

[12] W. J. Parker, R. J. Jenkins, C. P. Butler, and G. L. Abbott, "Flash method of determining thermal diffusivity, heat capacity, and thermal conductivity," *Journal of Applied Physics*, vol. 32, no. 9, pp. 1679–1684, 1961.